Eur. J. Biochem. **268**, 4653–4663 (2001) © FEBS 2001

Alternate routes to conformational specificity in a Greek key β barrel protein

Xiao-Fei Qi, Stefan Bagby*, Zoltan Gombos, Mitsuhiko Ikura and Avijit Chakrabartty

Division of Molecular and Structural Biology, Ontario Cancer Institute and Department of Medical Biophysics, University of Toronto, Ontario, Canada

The N-terminal domain of protein S, a Greek key calcium-binding protein from *Myxococcus xanthus*, forms an atypical molten globule in the calcium-free state. The structure of this state is characterized by significant conformational fluctuations, which are localized to a subdomain that is not contiguous along the polypeptide chain. The conformational instability of this subdomain appears to arise from repulsive electrostatic interactions of four acidic side chains that are clustered together but are removed from the calcium-binding sites. This domain can be induced to form a native-like state through two different routes, calcium binding or reduction of pH. Acid-induced folding stabilizes the locally unfolded subdomain by selectively removing repulsive interactions without significantly affecting global stability. In contrast, calcium binding appears to increase local stability indirectly by causing global stabilization.

Keywords: Greek key β barrel; protein folding intermediates; molten globule; calcium-dependent folding; acid-induced folding.

Molten globule states of proteins have been studied extensively to gain insights into the mechanisms by which native proteins attain conformational specificity and stability [1]. Similarities between the structural properties of molten globule states and kinetic folding intermediates [2–4] has led to the use of molten globule states as stable models for kinetic folding intermediates [5]. It is also becoming apparent that molten globule states of proteins are populated *in vivo* and may have physiological functions [6–8]. Elucidation of the structure and stabilizing interactions of proteins in their molten globule states is therefore of considerable importance.

Here we report structural studies on the molten globule state of the N-terminal domain of protein S (S-NTD). Protein S is a developmentally regulated, calcium-binding, Greek key protein, which forms a multilayer protective coat on the surface of myxospores of *Myxococcus xanthus*. Biosynthesis of protein S is induced by nutrient deprivation and the protein accumulates in the cytoplasm prior to secretion [9]. Protein S resembles the βγ-crystallins and is composed of two domains [10–12]. The isolated S-NTD comprising residues 2–92 is stable in isolation [13]. The X-ray crystal structure of a variant of S-NTD that is comprised of residues 2–89 reveals the presence of two bound calcium ions [14].

Correspondence to A. Chakrabartty, Division of Molecular and Structural Biology, Ontario Cancer Institute and Department of Medical Biophysics, University of Toronto, 610 University Avenue, Toronto, Ontario, Canada, M5G 2M9. Fax: + 416 946 6529, Tel.: + 416 946 2000 ext. 4910; E-mail: chakrab@uhnres.utoronto.ca

Abbreviations: S-NTD, N-terminal domain of protein S.

**Present address*: Department of Biology and Biochemistry, University of Bath, Bath, BA2 7AY, UK.

(Received 12 February 2001, revised 29 May 2001, accepted 4 July 2001)

Using NMR we have demonstrated previously that S-NTD can be divided into calcium-sensitive and calcium-insensitive subdomains, which are not contiguous along the polypeptide chain [15]. In the calcium-free state, the calcium-sensitive subdomain of S-NTD takes on molten globule characteristics while the calcium-insensitive subdomain remains native-like. Calcium binding restores the native state of S-NTD and causes a global stabilization of the structure. We now report that the calcium-sensitive subdomain of S-NTD can also be induced to form a native-like structure by lowering the pH. Interestingly, the acid-induced folding of this subdomain is mediated through different molecular interactions than calcium-induced folding and is accompanied by a loss of global structural stability. Thus, a native-like conformation of S-NTD can be attained through two different routes that differ in mechanism.

MATERIALS AND METHODS

Protein expression, purification, and NMR sample preparation

Protein S-NTD was overexpressed in *Escherichia coli* using a derivative of the pETlla plasmid carrying a phage T7 promoter, and was purified by $(NH_4)_2SO_4$ precipitation followed by ion-exchange chromatography. The purified protein homogeneity exceeded 95% as judged by SDS/PAGE and 2D NMR spectroscopy. Uniformly ^{15}N- and $^{15}N/^{13}C$-labeled protein for NMR experiments was obtained by using $^{15}NH_4Cl$ and $^{15}NH_4Cl/[^{13}C_6]$D-glucose as the sole nitrogen/carbon sources in M9 media. The ^{15}N- or $^{15}N/^{13}C$-labeled protein was dissolved in 95% H_2O/5% ^2H_2O at a concentration of 1.6 mM. The samples of calcium-bound protein contained 10 mM $CaCl_2$, 100 mM KCl, and 0.05 mM NaN_3. Samples of calcium-bound and calcium-free S-NTD were adjusted to the desired pH without correction for isotope effects. Details of S-NTD

expression, purification, and NMR sample preparation have been reported previously [15].

Circular dichroism spectroscopy

CD measurements were performed on an Aviv 62DS spectropolarimeter. Far-UV CD spectra were recorded in a 0.1-cm quartz cell in 2 mM Mes, 25 °C. The samples contained 20 μM protein S-NTD with either 10 mM $CaCl_2$ or 1 mM EDTA at pH 6.7, and 20 μM S-NTD with 1 mM EDTA at pH 2.6, respectively. Near-UV CD spectra were collected under the same conditions in a 1-cm quartz cell. Urea denaturation measurements, monitored at 218 nm, were recorded in a 1-cm quartz cell in 2 mM sodium phosphate or Mes, 25 °C. The samples contained 5.0 μM protein S-NTD with either 10 mM $CaCl_2$ or 1 mM EDTA at pH 6.7, and 5.0 μM protein S-NTD with 1 mM EDTA at pH 2.6. The concentration of urea varied between 0 and 8 M. CD measurements are reported as mean residue ellipticity [θ] at a given wavelength. Protein concentration in stock solutions was determined by dissolving aliquots in 6 M guanidine-HCl and measuring tyrosine absorbance at 275 nm, using 1450 $M^{-1} \cdot cm^{-1}$ as the extinction coefficient for a single tyrosine [16].

Ultraviolet-absorption spectroscopy

Urea denaturation, monitored by changes in tyrosine absorbance, was recorded in a 1-cm quartz cell in 2 mM sodium phosphate or Mes at 25 °C. The samples contained 100 μM S-NTD with either 10 mM $CaCl_2$ or 1 mM EDTA at pH 6.7, and 100 μM protein S-NTD with 1 mM EDTA at pH 2.6. The concentration of urea varied between 0 and 8 M. Changes in sample absorbance at 300, 286, and 264 nm were measured on a Milton Roy 3000 Diode Array Spectrophotometer. The difference in absorbance between 285 nm and 300 nm was divided by the difference in absorbance between 264 and 300 nm and this ratio was plotted against the urea concentration [17].

Measurement of calcium binding affinities

Ca^{2+} binding affinities were determined using the fluorescent chelator method, as described previously in detail [18,19]. Briefly, quin-2 (Molecular Probes, Eugene, OR, USA) was dissolved in 100 mM KCl, 2 mM Tris/HCl (pH 7.5) to a concentration of 23.86 μM (Molecular Probes). The Ca^{2+} concentration in the solution was below 2.0 μM. To remove Ca^{2+}, S-NTD was treated with EGTA, dialysed, and lyophilized. S-NTD was diluted in the quin-2 solution to a concentration of 25.2 μM. The concentrations were calculated by UV absorption. All titrations were carried out at room temperature using an acid-washed quartz cell with a 1-cm path length and were performed through the sequential addition of aliquots of 75 mM $CaCl_2$ (concentration determined by atomic absorption spectroscopy, University of Toronto, Toronto, ON, Canada) followed by absorbance measurements at 263 nm on an Ultrospec 2000 spectrophotometer. The macroscopic binding constants were calculated on the raw data by iterative least squares fit as described previously [18,19] using a custom-made fitting program (provided by S. Linse, University of Lund, Sweden). For S-NTD, fits using 1, 2, and 3 macroscopic binding constants were attempted.

NMR data acquisition

All NMR spectra were acquired at 30 °C on a Varian UNITY-plus 500 spectrometer operating at a proton frequency of 499.843 MHz and equipped with an actively shielded Z-gradient and a gradient amplifier unit. The carrier positions were used as follows: ^{13}CO, 176 p.p.m.; ^{15}N, 117.5 p.p.m.; $^{13}C^{\alpha}$, 58 p.p.m.; $^{13}C^{\alpha/\beta}$, 43 p.p.m.; ^{1}H, 4.725 p.p.m. (on resonance with the water frequency). When possible, NMR data were acquired using sensitivity enhancement [20,21] and pulsed-field gradients for coherence transfer pathway selection and artifact suppression [22,23]. Sensitivity was further improved by minimizing the degree of water saturation [24–27].

Two-dimensional $^{1}H–^{15}N$ HSQC spectra [28,29] were acquired with 128 complex points in t_1, 1024 complex points in t_2, and 16 transients. Triple-resonance spectra were recorded on uniformly $^{13}C/^{15}N$-labeled S-NTD with the following numbers of complex points and spectral widths: HNCO [30,31] ^{15}N (t_1) 32, 1464 Hz, ^{13}CO (t_2) 64, 1500 Hz, ^{1}H (t_3) 1024, 8000 Hz (24 transients); HNCACB [31,32], $^{13}C^{\alpha/\beta}$ (t_1) 48, 7625 Hz, ^{15}N (t_2) 28, 1464 Hz, ^{1}H (t_3) 1024, 8000 Hz (48 transients); CBCA(CO)NH [31] $^{13}C^{\alpha/\beta}$ (t_1) 48, 7625 Hz, ^{15}N (t_2) 28, 1464 Hz, ^{1}H (t_3) 1024, 8000 Hz (24 transients); (HB)CBCACO(CA)HA [31] $^{13}C^{\alpha/\beta}$ (t_1) 54, 7625Hz, ^{13}CO (t_2) 64, 1500 Hz, ^{1}H (t_3) 768, 6000 Hz (16 transients); HBHA(CBCACO)NH (L. E. Kay, University of Toronto, ON, Canada, personal communication) $^{1}H^{\alpha/\beta}$ (t_1) 50, 3000 Hz, ^{15}N (t_2) 32, 1464 Hz, ^{1}H (t_3) 1024, 8000 Hz (40 transients).

NMR spectra processing and resonance assignments

All spectra were processed and displayed using NMRPIPE, NMRDRAW [33], and NMRVIEW [34]. A 60° phase-shifted sine bell and single zero fill were typically applied prior to Fourier transformation in all dimensions of triple-resonance spectra. In the t_1 dimension of $^{1}H–^{15}N$ HSQC spectra, a 45° phase-shifted sine bell was applied prior to Fourier transformation, and a Lorentzian-to-Gaussian filter with NMRPIPE parameters G1 = 10 Hz (inverse exponential width), G2 = 20 Hz (Gaussian width), and G3 = 0 (corresponding to a maximum at the first point in the FID) was applied in the t_2 dimension. For the HNCACB, CBCA(CO)NH, HBHA(CBCACO)NH, and (HB)CBCACO(CA)HA data sets, linear prediction [35] was used to double the number of planes in the t_2 dimension. Where necessary, the residual water signal was reduced using a time-domain deconvolution approach [36]. Sequential resonance assignments were obtained from a combination of HNCACB, CBCA(CO)NH (HB) CBCACO(CA)HA, HBHA(CBCACO)NH, and HNCO spectra.

Calculation of electrostatic potential distribution

Electrostatic potential distribution on the surface of calcium-bound S-NTD at pH 6.7 was calculated according to the finite-difference Poisson–Boltzmann method using DELPHI [37,38] and displayed with INSIGHT II (Biosym

Technologies Inc.). The S-NTD coordinates were taken from the coordinate file of crystal structure of the S-NTD variant (RCSB PDB accession no. 1nps) [14]. The interior and exterior dielectric constants were set to 4 and 80, respectively. For the water solvent, both ionic strength and ionic radius were set to zero, and solvent radius was set to 1.4 Å. The protein surface is color coded by electrostatic potential values from the calculation.

RESULTS AND DISCUSSION

Effect of calcium and pH on the structure of S-NTD

Our previous NMR study showed that calcium-bound S-NTD at pH 6.7 possesses very similar chemical shifts to the N-terminal domain of full length protein S. This suggests that isolating the N-terminal domain has little effect on the overall structure of the domain [15] (Fig. 1C). This has since been confirmed by the elucidation of the X-ray crystal structure of a S-NTD variant that shows an overall backbone rmsd of 1.1 Å when compared with the N-terminal domain of the NMR structure of full-length protein S [14].

We had also shown that in the $^{1}H-^{15}N$ HSQC spectrum of calcium-free S-NTD at pH 6.7 (Fig. 1A), residues 1, 2, 6–18, 34–45, and 66–80 could not be sequentially assigned due to lack of signals. This region corresponds to the calcium-sensitive subdomain of S-NTD. The calcium-insensitive subdomain is comprised of the 47 residues that could be assigned. Thirty-four residues of the calcium-insensitive subdomain gave rise to two peaks in the $^{1}H-^{15}N$ HSQC spectrum of calcium-free S-NTD at pH 6.7 (Fig. 1A), indicating that the NH groups are undergoing slow exchange between two different states. As the chemical shifts of the doubled cross peaks are similar to the chemical shifts of the cross peaks in the $^{1}H-^{15}N$ HSQC spectrum of calcium-bound protein S-NTD (Fig. 1C), we proposed that these peak pairs arise from a two-state exchange involving the native state and a state with near-native structure [15]. When the pH was decreased to pH 2.6, however, the dispersion pattern and number of NH backbone cross peaks of S-NTD closely resembled calcium-bound S-NTD [15].

We have now performed three-dimensional triple-resonance NMR experiments to obtain NH, ^{15}N, $^{13}C^{\alpha}$, and $^{13}C^{\beta}$ backbone chemical shifts of the detectable resonances for calcium-free S-NTD at pH 2.6 (Table 1). As illustrated in the $^{1}H-^{15}N$ HSQC spectrum (Fig. 1B), 70 backbone amide cross peaks were assigned including residues 2–6, 9–19, 22–34, 36, 40–44, 47–63, 67–73, 79–87, 89–90. Due to the absence of signals, 14 backbone amide groups were not sequentially assigned (residues 7, 8, 35, 37–39, 64–66, 75–78, 92). However, of these residues with unassigned NH and ^{15}N groups, assignments were obtained for $^{13}C^{\alpha}$ and $^{13}C^{\beta}$ nuclei in residues 8, 35, 36, 39, 64, 78, and 91. Remarkably, the resonance NH cross peak of Arg92 was not visible in the $^{1}H-^{15}N$ HSQC spectrum at pH 2.6 but was present in the spectra of both calcium-bound and calcium-free S-NTD at pH 6.7 (Fig. 1A–C).

The average chemical shift changes of ^{1}NH, ^{15}N, $^{13}C^{\alpha}$, and $^{13}C^{\beta}$ nuclei between calcium-bound S-NTD at pH 6.7 and calcium-free S-NTD at pH 2.6 were calculated and are shown as a function of residue number in Fig. 2. Of the 70 assigned residues, 27 residues displayed significant changes in chemical shift (0.2–1.6 p.p.m.). These residues with large chemical shift changes are sequentially close to unassigned regions of the sequence and they may represent boundaries of dynamic regions of calcium-free S-NTD at pH 2.6. Some of the changes in chemical shift may also arise from differences in solvent conditions between NMR samples.

The effects of calcium and pH on the secondary structure of S-NTD were evaluated using NMR chemical shift indices [39–42]. The values of chemical shift indices were calculated from all assigned $^{13}C^{\alpha}$ and $^{13}C^{\beta}$ resonances. Indices for calcium-free S-NTD at both pH 2.6 and pH 6.7

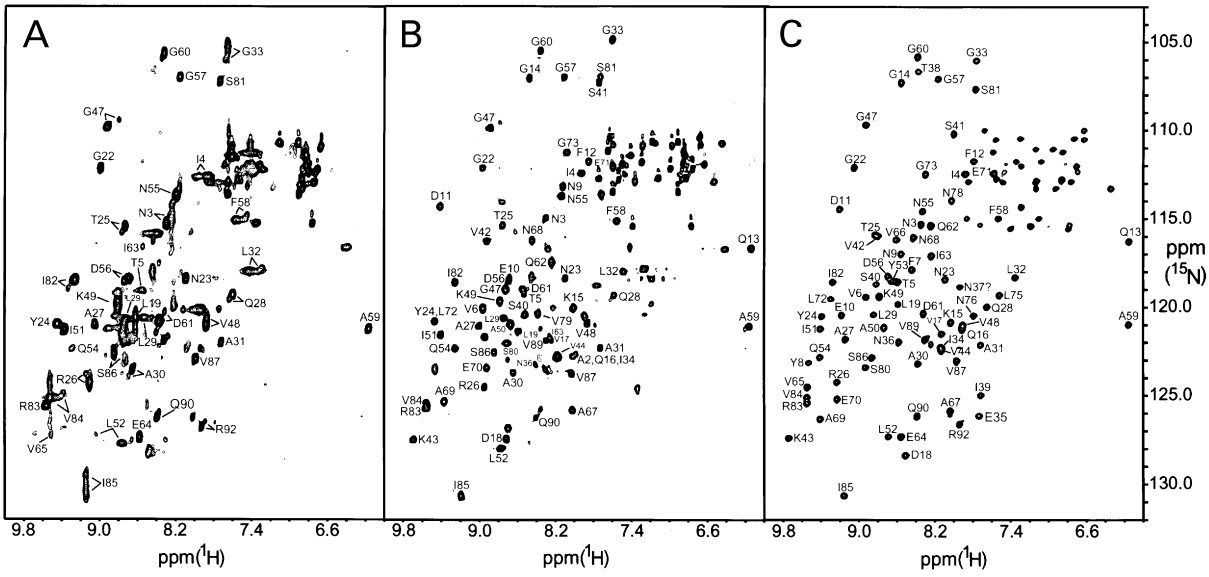

Fig. 1. $^{1}H-^{15}N$ HSQC spectra of protein S-NTD. (A) Calcium-free protein S-NTD, pH 6.7; (B) calcium-free protein S-NTD, pH 2.6; (C) calcium-bound protein S-NTD, pH 6.7. Peaks are labeled with the one-letter amino acid code and sequence position of the amino-acid residue.

Table 1. ^{15}N, $^{13}C^{\alpha}$, $^{13}C^{\beta}$, ^{13}CO, NH and H^{α} assignments for protein S-NTD at pH 2.6.

Residue	^{15}N (NH)	CO	C^{α} (H^{α})	C^{β}
M1				
A2	122.7 (8.02)	171.60	52.8 (4.02)	19.300
N3	114.9 (8.29)	176.80	51.9 (5.11)	40.700
I4	112.5 (7.94)	176.10	60.5 (4.89)	39.600
T5	119.0 (8.55)	173.50	62.1 (5.05)	71.000
V6	120.2 (8.96)		60.7	33.000
F7				
Y8		176.10	59.9 (4.89)	40.100
N9	112.9 (8.14)	175.30	51.3 (5.13)	42.000
E10	118.5 (8.67)	176.00	56.3 (3.73)	28.800
D11	114.3 (9.42)	173.20	53.9 (3.17)	36.400
F12	111.7 (7.86)	173.80	55.1 (2.51)	35.700
Q13	116.7 (6.14)	175.10	53.7 (4.69)	32.400
G14	107.1 (8.48)	173.50	44.4 (4.97)	
K15	120.1 (8.00)	175.30	57.9 (3.97)	32.800
N16	122.7 (7.99)	175.00	52.4 (4.44)	32.500
V17	121.6 (8.26)	174.00	61.6 (4.12)	36.700
D18	127.4 (8.73)	174.30	52.2 (5.40)	39.800
L19	121.5 (8.59)		52.0	44.400
P20				
P21		175.60	64.4 (4.17)	31.800
G22	112.1 (8.97)	182.30	44.7 (4.05, 3.77)	
N23	118.3 (8.09)	173.90	52.5 (5.26)	40.700
Y24	120.8 (9.48)	175.10	57.3 (5.14)	41.100
T25	115.3 (8.76)	174.30	60.7 (4.15)	71.300
R26	124.5 (8.91)	179.60	60.8 (4.48)	30.400
A27	121.0 (8.97)	181.80	55.0 (4.19)	18.500
Q28	119.3 (7.59)	179.40	58.9 (4.20)	29.600
L29	120.6 (8.73)	179.50	58.0 (3.97)	40.200
A30	123.7 (8.66)	182.40	54.9 (4.34)	17.600
A31	122.3 (7.73)	179.40	54.8 (4.21)	18.100
L32	118.0 (7.49)	176.80	55.0 (4.35)	42.600
G33	104.8 (7.60)	174.50	44.9 (4.25, 3.83)	
I34	122.8 (8.04)		60.5	36.100
E35				
N36	122.9 (8.45)		56.0	30.400
N37				
T38				
I39		175.30	61.4 (4.35)	34.500
S40	120.2 (8.50)	171.90	59.5 (4.67)	66.000
S41	107.3 (7.75)	173.80	59.2 (4.26)	65.300
V42	116.3 (8.92)	174.00	60.3 (5.99)	36.400
K43	127.5 (9.68)	175.40	56.0 (4.63)	35.600
V44	122.6 (8.18)		64.3	33.500
P45				
P46		178.00	63.5 (4.42)	31.900
G47	109.9 (8.88)	174.70	45.0 (4.26, 3.83)	
V48	120.8 (7.86)	171.90	59.7 (5.12)	36.500
K49	119.7 (8.79)	173.40	54.7 (4.78)	36.900
A50	121.0 (8.66)	175.00	50.4 (5.71)	23.600
L51	121.6 (9.41)	173.90	61.2 (4.68)	39.300
L52	128.0 (8.79)	174.50	54.5 (4.42)	42.600
Y53	119.0 (8.73)	176.80	57.1 (5.10)	40.000
Q54	122.4 (9.25)	176.60	57.4 (4.68)	31.300
N55	113.8 (8.15)	175.50	50.8 (5.18)	40.400
D56	118.6 (8.70)	176.70	53.1 (4.25)	40.700
G57	107.0 (8.09)	174.30	46.6 (2.97)	
F58	111.5 (7.54)	173.80	56.0 (2.45)	35.200
A59	121.1 (6.17)	175.70	50.4 (4.79)	22.800
G60	105.5 (8.35)	174.10	44.2 (4.39, 3.82)	

Table 1. continued.

Residue	^{15}N (NH)	CO	C^{α} (H^{α})	C^{β}
D61	119.1 (8.54)	173.60	54.3 (4.59)	37.900
Q62	117.4 (8.26)	175.00	52.4 (5.29)	32.500
I63	121.6 (8.26)	176.00	61.8	36.700
E64				
V65				
V66		174.50	59.7 (4.69)	32.400
A67	125.8 (8.03)	175.00	50.8 (4.66)	22.000
N68	116.3 (8.44)	175.60	54.4 (4.32)	38.500
A69	125.2 (9.36)	176.10	51.1 (5.03)	20.800
E70	123.4 (8.92)	173.70	58.6 (3.29)	28.800
E71	112.0 (7.60)		54.5	31.700
L72	120.7 (9.47)	177.60	52.6 (5.10)	41.300
G73	111.2 (8.09)		47.0	
P74				
L75				
N76				
N77				
N78		174.00	58.9 (4.75)	32.700
V79	120.5 (8.39)	176.90	56.7 (5.46)	41.100
S80	122.0 (8.71)	172.50	59.4 (4.97)	66.600
S81	106.9 (7.73)	173.60	49.2 (4.27)	65.300
I82	118.7 (9.27)	175.20	61.2 (5.63)	45.900
R83	125.8 (9.58)	174.80	56.1 (5.36)	33.200
V84	125.4 (9.56)	175.90	62.8 (4.05)	33.200
I85	130.5 (9.20)	174.90	60.5 (4.40)	42.400
S86	122.5 (8.85)	174.00	59.2 (4.76)	63.500
V87	123.7 (8.04)		58.8	33.400
P88		177.10	62.8 (4.44)	32.000
V89	121.9 (8.30)	176.20	62.5 (4.04)	32.600
Q90	126.2 (8.40)		53.5	29.200
P91				
R92				

are highly similar to those for calcium-bound S-NTD at pH 6.7 (Fig. 3A–C). Thus, even at the level of individual residues, the secondary structure of assigned regions of calcium-free S-NTD at pH 2.6 is similar to the secondary structure of calcium-bound S-NTD at pH 6.7. This result was confirmed by CD measurements, which showed that far-UV CD spectra of calcium-free S-NTD at pH 2.6 and pH 6.7 and calcium-bound S-NTD are virtually superimposable (Fig. 4A). The near-UV CD spectra of these states, on the other hand, are considerably different from one another. The near-UV CD bands of calcium-bound S-NTD are all negative and become displaced progressively to more positive values in calcium-free S-NTD at pH 6.7 and pH 2.6, respectively (Fig. 4B). These differences in near-UV CD may result from changes in the electronic environment of aromatic residues associated with removal of calcium and reduction in pH as much as from changes in tertiary structure. Given the similarities of the ^{1}H–^{15}N HSQC spectra of calcium-free S-NTD, pH 2.6 and calcium-bound S-NTD, it is possible that the differences in near-UV CD spectra result mostly from changes in solvent conditions rather than changes in tertiary structure.

We also examined the effect of calcium and pH on the ability of S-NTD to bind the hydrophobic dye 8-anilinonaphthalene-1-sulfonate. 8-Anilinonaphthalene-1-sulfonate

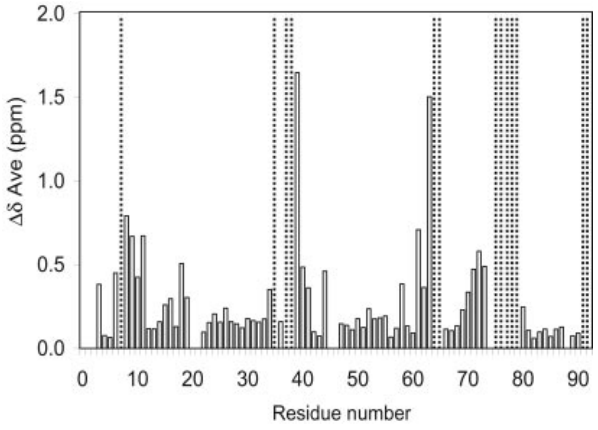

Fig. 2. The average chemical shift changes (Δ_{Ave}) of ^{1}HN, ^{15}N, $^{13}C^{\alpha}$ and $^{13}C^{\beta}$ between calcium-bound protein S-NTD at pH 6.7 and calcium-free protein S-NTD at pH 2.6 as a function of residue number. The average change in chemical shift was calculated as $[(\Delta\delta^2_{NH} + \Delta\delta^2_{N}/25 + \Delta\delta^2_{C\alpha}/4 + \Delta\delta^2_{C\beta}/4)/4]^{1/2}$. Dotted lines indicate those residues for which sequential resonance in calcium-free protein S-NTD at pH 2.6 could not be obtained due to conformational flexibility. The average chemical shift change for Pro residues could not be calculated.

fluorescence was greatest in the presence of calcium-free S-NTD at pH 6.7; however, either in the presence of calcium or at pH 2.6, 8-anilinonaphthalene-1-sulfonate fluorescence was greatly diminished (data not shown). As 8-anilinonaphthalene-1-sulfonate fluorescence increases when the dye is sequestered in hydrophobic environment, these results indicate that hydrophobic groups which are buried in either calcium-bound S-NTD at pH 6.7 or calcium-free S-NTD at pH 2.6, are exposed in calcium-free S-NTD at pH 6.7.

From the NMR and optical spectroscopy experiments discussed above, a qualitative assessment of the calcium- and pH-induced changes in structure is possible. As we described previously, calcium-free S-NTD at pH 6.7 adopts an unusual molten globule structure in which the calcium-sensitive subdomain shows intermediate timescale conformational fluctuations and the calcium insensitive subdomain is in slow exchange between native and near-native conformations [15]. We now show that calcium-free S-NTD at pH 2.6 possesses significantly greater native-like characteristics. The slow conformational exchange process and 8-anilinonaphthalene-1-sulfonate-binding have disappeared, and the majority of the residues have chemical shifts that are similar to calcium-bound S-NTD. The secondary structure of calcium-free S-NTD at pH 2.6 closely matches that of calcium-bound S-NTD, even at the level of individual residues. However, missing assignments at residues 7, 37, 38, 65, 66, 75–77, and 92 indicates conformational instability in these regions. It should be noted that residues 33–40 and 72–80 of both calcium-bound S-NTD [15] and calcium-bound full-length protein S [43] probably constitute the most unstable regions based on the relatively low intensity, or in many cases, absence of NMR signals.

Effect of calcium and pH on conformational stability of S-NTD

The stabilities of calcium-free S-NTD at pH 6.7 and 2.6 were assessed by urea denaturation experiments monitored by changes in CD at 218 nm and by changes in tyrosine absorbance. After normalization, the denaturation curves obtained from CD and tyrosine absorbance measurements were superimposable (Fig. 5B,C) suggesting that calcium-free S-NTD at pH 6.7 and 2.6 display cooperative two-state unfolding transitions [44]. The folding free energies for calcium-free S-NTD at pH 6.7 and 2.6 are -25 and -19 kJ·mol^{-1}, respectively (Table 2). This result is surprising given that calcium-free S-NTD at pH 6.7 possesses molten globule characteristics while calcium-free S-NTD at pH 2.6 is native-like. In addition, the preponderance of acidic residues in S-NTD would predict a low isoelectric point, ≈ 4. Consequently, the net charge on S-NTD at pH 2.6 could be of similar or lesser magnitude than that at pH 6.7. Thus, electrostatic repulsion may not be responsible for the lower stability of the low pH form of S-NTD. One possibility is the presence of a stabilizing salt bridge interaction in the pH 6.7 form of S-NTD, which gets disrupted at pH 2.6. A single salt bridge has been observed between Lys49 and Glu64 of the crystal structure of the S-NTD variant [14]; however, this salt bridge is solvent exposed and Glu64 also interacts with neighboring molecules in the crystal lattice. Thus, the stabilizing influence of this interaction is questionable. Another explanation for the greater stability of the molten globule form of calcium-free S-NTD at pH 6.7 relative to the native-like form at pH 2.6 is that less conformational entropy is lost in forming the molten globule state than the native-like state.

Urea denaturation experiments of calcium-bound S-NTD were attempted; however, this form of S-NTD was highly resistant to denaturation and complete unfolding did not occur, even at 8 M urea concentration (Fig. 5A). Calcium binding thus appears to stabilize S-NTD significantly.

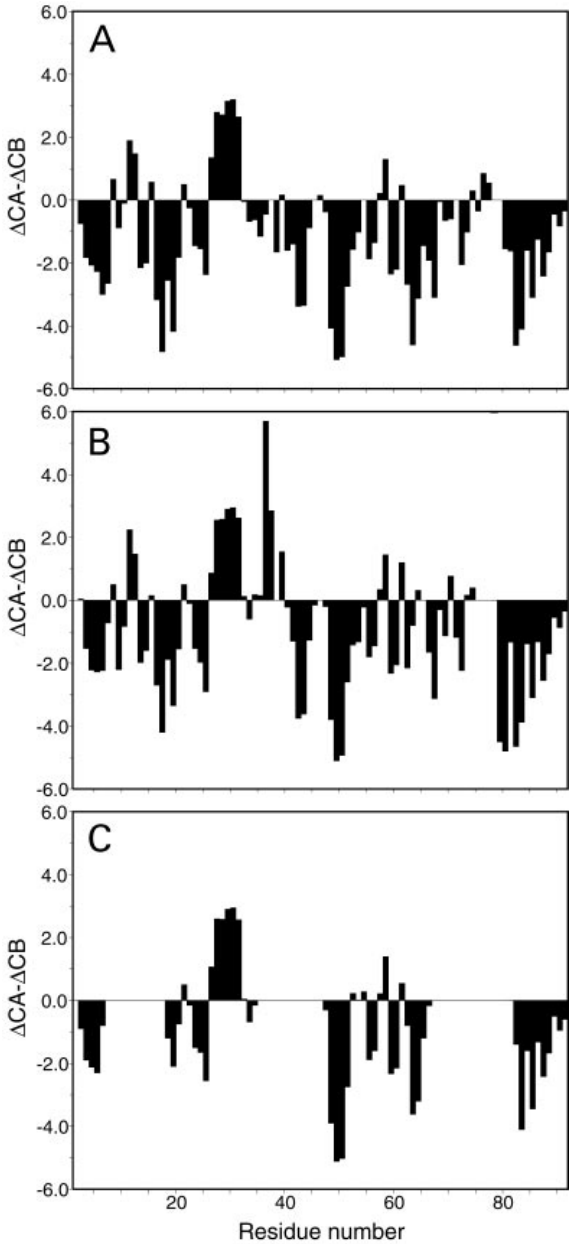

Fig. 3. The inferred secondary structures of calcium-bound protein S-NTD at pH 6.7 (A), calcium-free protein S-NTD at pH 2.6 (B), and calcium-free protein S-NTD at pH 6.7 (C) from the chemical shift changes using $\Delta^{13}C^{\alpha}-\Delta^{13}C^{\beta}$ as a function of residue number. Possible helical and β sheet regions are indicated as positive and negative values of $\Delta^{13}C^{\alpha}-\Delta^{13}C^{\beta}$, respectively.

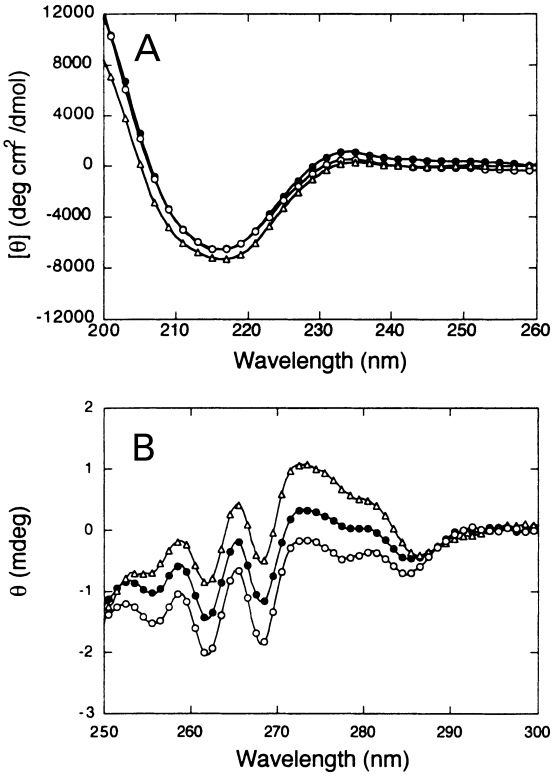

Fig. 4. Far-UV (A) and near-UV (B) CD spectra of calcium-bound protein S-NTD at pH 6.7 (○), calcium-free protein S-NTD at pH 6.7 (●) and at pH 2.6 (△).

The urea denaturation experiments reported here were modelled after the urea denaturation study of Wenk *et al.* [14] who examined a variant of S-NTD that lacked the last three amino-acid residues of S-NTD (Gln90, Pro91 and Arg92). As discussed above, the X-ray crystal structure of the variant is very similar to the structure of the N-terminal domain of full-length protein S; however, it has very different denaturation properties than S-NTD. While the calcium-free form of the S-NTD and the variant are similar with respect to the two-state folding mechanism, folding free energies, *m* values and denaturation midpoints [14,17,45,46], the remarkable calcium-induced stabilization that we observed with S-NTD was not observed with the variant. Apparently, the calcium-dependent stability of S-NTD is attributable to Gln90, Pro91, and Arg92. The structural basis of this effect is not clear in the NMR structure of full-length protein S. Gln90, Pro91, and Arg92 are solvent exposed and not involved in long–range interactions.

Calcium-binding properties of S-NTD

The X-ray crystal structure of the S-NTD variant revealed the presence of two bound calcium ions [14]. The first calcium ion is liganded by the side chain oxygen atoms of Ser80 and Asn37, and the backbone carbonyl oxygen atoms of Gln54 and and Asn78. The second calcium ion is liganded by the side chain oxygen atoms of Ser40 and Asn77, and the backbone carbonyl oxygen atoms of Thr38 and and Tyr8. To ensure that similar calcium-binding sites are present in S-NTD, we examined its calcium-binding properties using the chromophoric calcium chelator, quin-2. Consistent with the X-ray crystal structure, the calcium titration experiments suggested the presence of two calcium-binding sites with affinities of 12.5 nM and 154 nM (Fig. 6). The calcium-binding affinities of calmodulin were also determined as a control (data not shown). For calmodulin, four macroscopic calcium-binding sites with respective affinities of 12, 168, 310, and 549 nM produced the best fit, in agreement with previous results [18].

The calcium-binding affinities of S-NTD are very high compared to full-length protein S, which has calcium-binding affinities ≈ 27 and 76 μM under similar conditions [47]. One scenario that provides a possible explanation for this large difference is that the free energy of the calcium-bound form of S-NTD is similar to that of the N-terminal domain of full length protein S; however, the calcium-free form of S-NTD may have significantly lower free energy than the N-terminal domain of full length protein S. Support for this idea comes from our observation of the

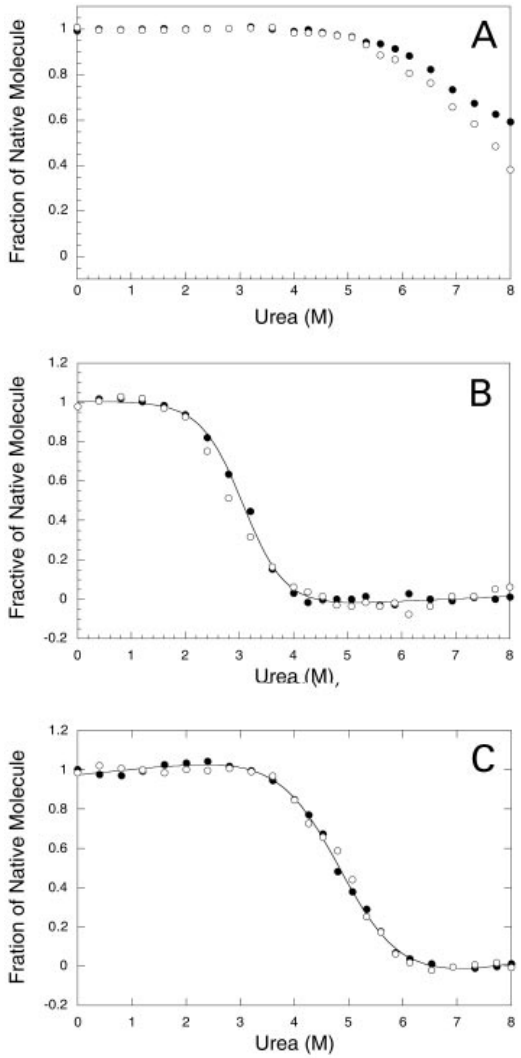

Fig. 5. Urea denaturation of (A) calcium-bound protein S-NTD at pH 6.7 (B) calcium-free protein S-NTD at pH 2.6, and (C) at pH 6.7, measured by absorption (●) and far-UV CD (○) at 25 °C.

Table 2. Stablity parameters of S-NTD from urea denaturation experiments at 25 °C. ND, not determined.

Solution conditions	$[Urea]_{1/2}$ [a] (M)	ΔG [b] ($kJ \cdot mol^{-1}$)	m [c] ($kJ \cdot mol^{-1} \cdot M^{-1}$)
pH 6.7			
$+Ca^{2+}$	> 8	ND	ND
$-Ca^{2+}$	4.8 ± 0.1	−25 ± 1	−5.0 ± 0.1
pH 2.6			
$-Ca^{2+}$	2.8 ± 0.1	−19 ± 1	−6.4 ± 0.3

[a] The midpoint of urea unfolding curve. [b] The calculated free energy change derived from linear extrapolation model. [c] Cooperativity of urea denaturation curve.

large enhancement of conformational stability of S-NTD upon calcium binding (Fig. 5).

Electrostatic charge distribution on the surface of S-NTD

To better understand the large effects of pH and calcium on the structure of S-NTD, we examined the electrostatic charge distribution on the surface of S-NTD in relation to the calcium-binding sites. We calculated electrostatic potential distribution on the surface of calcium-loaded S-NTD at pH 6.7 according to the finite-difference Poisson–Boltzmann method using the DELPHI program [37,38]. The coordinates were taken from the coordinate file of crystal structure of the S-NTD variant (RCSB PDB accession no. 1nps) [14]. The calculated results were displayed with INSIGHT II, which gives a graphical representation of the electrostatic properties of molecular surface (Fig. 7). In Fig. 7, the electrostatic charge distribution is compared with the location of the calcium-binding sites and the calcium-sensitive subdomain of S-NTD.

The most striking feature of the electrostatic surface of S-NTD is a concentrated region of extremely highly negative electrostatic potential. This negative potential arises from the clustering of the acidic residues: Glu10, Asp11, Glu70, and Glu71. The location of this region is highly correlated with the calcium-sensitive subdomain. This very close correspondence implicates repulsive interactions between clustered acidic side chains as the cause of molten globule behavior of this subdomain. One puzzling aspect of this observation is that the repulsive forces cause local unfolding but not global destabilization. If the repulsive forces caused global destabilization, then attenuation of the negative charge through pH titration should increase the stability of calcium-free S-NTD. Instead, we observed that S-NTD at pH 2.6 is less stable than at pH 6.7 (Table 2).

While there is superimposition of the calcium-sensitive subdomain with the region of very high negative electrostatic potential, the calcium-binding sites are slightly removed from this region. Thus, calcium binding does not directly screen repulsive interactions between clustered acidic side chains. Instead, it appears that the calcium-binding energy is distributed throughout the network of noncovalent interactions in S-NTD stabilizing the entire molecule as well as the locally unfolded calcium-sensitive subdomain. The free calcium concentration (10 mM) in the samples of calcium-bound S-NTD is too low to screen the unfavorable charge repulsion between the clustered carboxylate groups.

The distribution of electrostatic potential on the surface of S-NTD pinpoints the potential cause of local instability in the calcium-sensitive subdomain as being repulsive interactions between clustered acidic side chains. While both calcium- and acid-induced folding alleviate the local instability, they utilize different mechanisms. Whereas acid-induced folding selectively removes the repulsive interactions, calcium binding increases local stability indirectly by causing global stabilization.

Comparison with other work

The molten globule state of calcium-free S-NTD is atypical in its stability and structure. Molten globule forms of other proteins, such as apomyoglobin [48], α-lactalbumin [49], and ribonuclease H [50], are much less structured. For example, the molten globule state of apomyoglobin is comprised of a partially stable core composed of helices A, G, and H and a small segment of helix B; all of core helices display conformational dynamics such as fraying from the ends [51]. Unstable but measurable helical structure is present in helices C, D, and E, while the F helix segment is unstructured. A number of specific tertiary interactions appear to be present in the core, but native-like packing is not observed [52].

The molten globule state of α-lactalbumin displays even greater fluctuations in structure, and its constituent helices can be individually unfolded with proline mutations

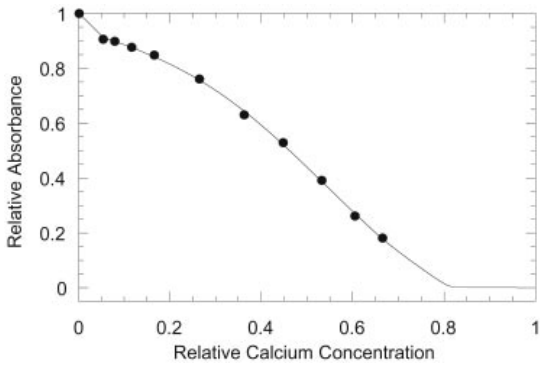

Fig. 6. Calcium titrations in the presence of quin-2. Normalized absorbance measurements are plotted against normalized calcium concentrations. Experimental points for S-NTD using quin-2 as the indicator dye, pH 7.5. The curve is a best-fit line employing different binding models. A model employing two macroscopic calcium-binding constants of 12.5 and 154 nM produced the best fit.

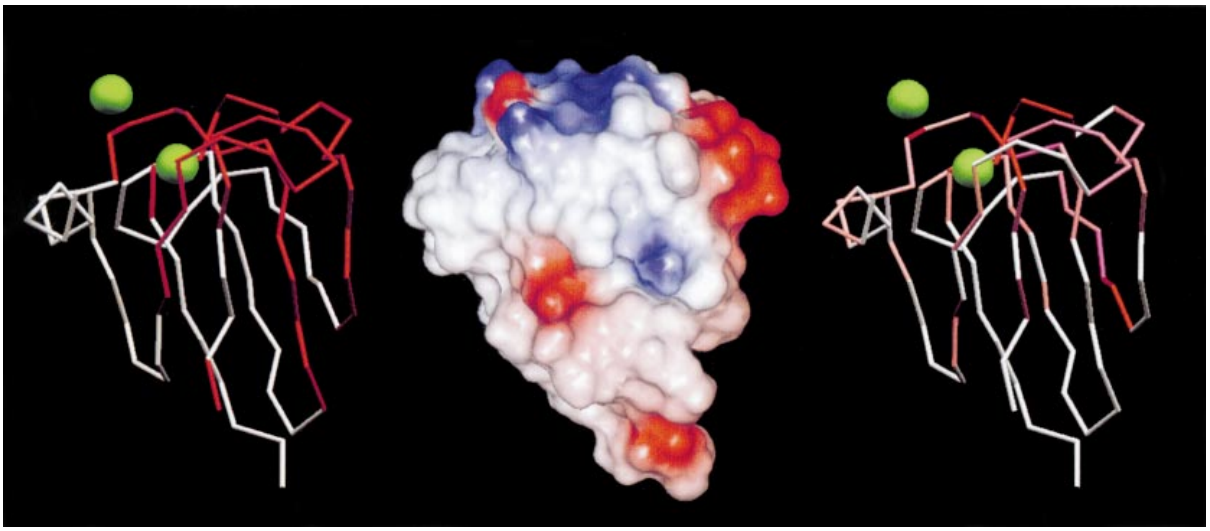

Fig. 7. The α-carbon trace representation of three-dimensional structure of S-NTD at pH 6.7 (left), the electrostatic charge distribution on the surface of calcium-bound S-NTD in aqueous solution (center), and the α-carbon trace of S-NTD superimposed with the average differences in chemical shift between calcium-free S-NTD at pH 2.6 and calcium-bound S-NTD at pH 6.7 (right). (Left) Red indicates the calcium-sensitive subdomain, i.e. residues for which sequential resonance assignments could not be obtained due to conformational flexibility. White indicates the calcium-insensitive subdomain, i.e. assignable residues in calcium-free at pH 6.7. (Center) The electrostatic charge distribution on the surface of calcium-bound S-NTD in aqueous solution. Positive potential values are blue, negative values are red, and neutral potential values are white. Linear interpolation was used to produce the color for surface potentials between these values. The calcium-sensitive subdomain is clearly distinguishable as a region of intense negative potential. (Right) The α-carbon trace of S-NTD superimposed with the average differences in chemical shift between calcium-free S-NTD at pH 2.6 and calcium-bound S-NTD at pH 6.7. Red indicates a value of $\Delta_{ave} = 1.65$ p.p.m., white indicates $\Delta_{ave} = 0$ p.p.m., and linear interpolation was used to produce the intermediate values. It can be seen that the largest chemical shift changes are localized mostly to the calcium-sensitive subdomain.

without affecting the rest of the structure [53]. However, the native topology and some specific tertiary interactions are still present [54]. The stability of this molten globule is thought to be derived from dehydration of the hydrophobic core without the formation of closely packed van der Waals interactions; an energetic consequence is an absence of heat absorption or production during calorimetric analysis [55]. In contrast, unfolding of the calcium-free form of S-NTD variant is accompanied by an easily measurable positive enthalpy and heat capacity change [46]. The molten globule state of S-NTD appears to be more closely related to that of canine milk lysozyme, which shows a measurable enthalpy and heat capacity change upon unfolding as well as resolvable resonances in NMR spectra [56].

Another unusual feature of S-NTD is that its molten globule state is most populated at neutral pH and is diminished at acid pH. In contrast, there are many examples of proteins that form molten globules or A-states at acid pH [57]. Acid-induced formation of A-states is attributed to an increased need to hydrate positive charges and maximize their separation distance. Acidifying S-NTD, on the other hand, neutralizes a cluster of four negatively charged groups and permits them to associate and form the native state. S-NTD thus does not display disparate behavior from A-state forming proteins. Taken together, the results of S-NTD and the A-state proteins indicate that molten globule formation is a response to the local buildup of unfavorable charge, be it positive or negative.

ACKNOWLEDGEMENTS

We thank D. L. S. Laurents for helpful discussion and S. Inouye for providing the S-NTD expresion vector. We thank S. Linse for providing the computer program for fitting data from the fluorescent chelator method. This work was supported by a grant to A. C. from the Canadian Institutes of Health Research (CIHR), and by a grant to M. I. from the National Cancer Institute of Canada. M. I. is an CIHR Scientist and a Howard Hughes Medical Institute International Scholar. Z. G. holds a Doctoral Research Award from CIHR.

REFERENCES

1. Kuwajima, K. (1989) The molten globule state as a clue for understanding the folding and cooperativity of globular protein structure. *Proteins* **6**, 87–103.
2. Jennings, P.A. & Wright, P.E. (1993) Formation of a molten globule intermediate early in the kinetic folding pathway of apomyoglobin. *Science* **262**, 892–896.
3. Arai, M. & Kuwajima, K. (1996) Rapid formation of a molten globule intermediate in refolding of alpha-lactalbumin. *Fold. Des.* **1**, 275–287.
4. Goedleen, E.R., Raschke, T.M. & Marqusee, S. (1997) Importance of the C-terminal helix to the stability and enzymatic activity of *Escherichia coli* ribonuclease H. *Biochemistry* **36**, 7256–7263.
5. Roder, H. & Colon, W. (1997) Kinetic role of early intermediates in protein folding. *Curr. Opin. Struct. Biol.* **7**, 15–28.
6. Bychkova, V.E., Pain, R.H. & Ptitsyn, O.B. (1988) The 'molten

globule' state is involved in the translocation of proteins across membranes? *FEBS Lett.* **238**, 231–234.
7. Ptitsyn, O.B., Bychkova, V.E. & Uversky, V.N. (1995) Kinetic and equilibrium folding intermediates. *Phil. Trans. R. Soc. Lond. B.* **348**, 35–41.
8. Wright, P.E. & Dyson, H.J. (1999) Intrinsically unstructured proteins: re-assessing the protein structure–function paradigm. *J. Mol. Biol.* **293**, 321–331.
9. Inouye, M., Inouye, S. & Zusman, D.R. (1979) Biosynthesis and self-assembly of protein S, a development-specific protein of *Myxococcus xanthus*. *Proc. Natl Acad. Sci. USA* **76**, 209–213.
10. Wistow, G., Summers, L. & Blundell, T. (1985) *Myxococcus xanthus* spore coat protein S may have a similar structure to vertebrate lens βγ-crystallins. *Nature.* **315**, 771–773.
11. Bagby, S., Harvey, T.S., Eagle, S.G., Inouye, S. & Ikura, M. (1994) NMR-derived three-dimensional solution structure of protein S complexed with calcium. *Structure* **2**, 107–122.
12. Bagby, S., Harvey, T.S., Eagle, S.G., Inouye, S. & Ikura, M. (1994) Structural similarity of a developmentally regulated bacterial spore coat protein to βγ-crystallins of the vertebrate eye lens. *Proc. Natl Acad. Sci. USA* **91**, 4308–4312.
13. Inouye, S., Franceschini, T. & Inouye, M. (1983) Structural similarities between the development-specific protein S from a gram-negative bacterium, *Myxococcus xanthus*, and calmodulin. *Proc. Natl Acad. Sci. USA* **80**, 6829–6833.
14. Wenk, M., Baumgartner, R., Holak, T.A., Huber, R., Jaenicke, R. & Mayr, E.M. (1999) The domains of protein S from *Myxococcus xanthus*: structure, stability and interactions. *J. Mol. Biol.* **286**, 1533–1545.
15. Bagby, S., Go, S., Inouye, S., Ikura, M. & Chakrabatty, A. (1998) Equilibrium folding intermediates of a Greek key β-barrel protein. *J. Mol. Biol.* **276**, 669–681.
16. Brandts, J.F. & Kaplan, L.J. (1973) Derivative spectroscopy applied to tyrosyl chromophores. Studies on ribonuclease, lima bean inhibitors, insulin, and pancreatic trypsin inhibitor. *Biochemistry* **12**, 2011–2024.
17. Wenk, M. & Mayr, E.M. (1998) *Myxococcus xanthus* spore coat protein S, a stress-induced member of the betagamma-crystallin superfamily, gains stability from binding of calcium ions. *Eur. J. Biochem.* **255**, 604–610.
18. Linse, S., Helmersson, A. & Forsen, S. (1991) Calcium binding to calmodulin and its globular domains. *J. Biol. Chem.* **266**, 8050–8054.
19. Linse, S., Johansson, C., Brodin, P., Grundstrom, T., Drakenberg, T. & Forsen, S. (1991) Electrostatic contributions to the binding of Ca^{2+} in calbindin D_{9k}. *Biochemistry* **30**, 154–162.
20. Cavanagh, I. & Rance, M. (1990) Sensitivity improvement in isotropic mixing (TOSCY) experiments. *J. Magn. Reson.* **88**, 77–85.
21. Kay, L.E., Keifer, P. & Saarinen, T. (1992) Pure absorption gradient enhanced heteronuclear single quantum correlation spectroscopy with improved sensitivity. *J. Am. Chem. Soc.* **114**, 10663–10665.
22. Kay, L.E. (1995) Field gradient techniques in NMR spectroscopy. *Curr. Opin. Struct. Biol.* **5**, 674–681.
23. Keeler, J., Clowes, R.T., Davis, A.L. & Laue, E.D. (1994) Pulsed-field gradients: theory and practice. *Methods Enzymol.* **239**, 145–207.
24. Grzesiek, S. & Bax, A. (1993) The importance of not saturating H_2O in protein NMR. Application to sensitivity enhancement and NOE measurements. *J. Am. Chem. Soc.* **115**, 12593–12594.
25. Kay, L.E., Xu, G.Y. & Yamazaki, T. (1994) Enhanced-sensitivity triple-resonance spectroscopy with minimal H_2O saturation. *J. Magn. Reson. A* **109**, 129–133.
26. Li, Y.-C. & Montelione, G.T. (1993) Solvent saturation-transfer effects in pulsed-field gradient heteronuclear single-quantum-coherence (PFG-HSQC) spectra of polypeptides and proteins. *J. Magn. Reson. B* **101**, 315–319.
27. Stonehouse, J., Shaw, G.L., Keeler, J. & Laue, E.D. (1994) Minimizing sensitivity losses in gradient-selected ^{15}N-^{1}H HSQC spectra of proteins. *J. Magn. Reson. A* **107**, 178–184.
28. Bodenhausen, G. & Ruben, D.J. (1979) Natural abundance nitrogen-15 NMR by enhanced heteronuclear spectroscopy. *Chem. Phys. Lett.* **69**, 185–189.
29. Zhang, O., Kay, L.E., Olivier, J.P. & Forman-Kay, J.D. (1994) Backbone ^{1}H and ^{15}N resonance assignments of the N-terminal SH3 domain of drk in folded and unfolded states using enhanced-sensitivity pulsed field gradient NMR techniques. *J. Biomol. NMR* **4**, 845–858.
30. Kay, L.E., Ikura, M., Tschudin, R. & Bax, A. (1990) Three-dimensional triple-resonance NMR spectroscopy of isotopically enriched proteins. *J. Magn. Reson.* **89**, 496–514.
31. Muhandiram, D.R. & Kay, L.E. (1994) Gradient-enhanced triple-resonance three-dimensional NMR experiments with improved sensitivity. *J. Magn. Reson. B* **103**, 203–216.
32. Wittekind, M. & Mueller, L. (1993) HNCACB, a high-sensitivity 3D NMR experiment to correlate amide-proton and nitrogen resonances with the alpha- and beta-carbon resonances in proteins. *J. Magn. Reson. B* **101**, 201–205.
33. Delaglio, F., Grzesiek, S., Vuister, G.W., Zhu, G., Pfeifer, J. & Bax, A. (1995) NMRPipe: a multidimensional spectral processing system based on UNIX pipes. *J. Biomol. NMR* **6**, 277–293.
34. Johnson, B.A. & Blevins, R.A. (1994) NMRView: a computer program for the visualization and analysis of NMR data. *J. Biomol. NMR* **4**, 603–614.
35. Barkhuijsen, H., De Beer, R., Bovee, W.M.M.J. & van Ormondt, D. (1985) Retrieval of frequencies, amplitudes, damping factors, and phases from time-domain signals using a linear least-squares procedure. *J. Magn. Reson.* **61**, 465–481.
36. Marion, D., Ikura, M. & Bax, A. (1989) Improved solvent suppression in one- and two-dimensional NMR spectra by convolution of time-domain data. *J. Magn. Reson.* **84**, 425–430.
37. Honig, B. & Nicholls, A. (1995) Classical electrostatics in biology and chemistry. *Science* **268**, 1144–1149.
38. Gilson, M., Sharpe, J. & Honig, B. (1988) Calculating the electrostatic potential of molecules in solution: method and error assessment. *J. Comp. Chem.* **9**, 327–335.
39. Wishart, D.S. & Sykes, B.D. (1994) The ^{13}C chemical-shift index: a simple method for the identification of protein secondary structure using ^{13}C chemical-shift data. *J. Biomol. NMR* **4**, 171–180.
40. Wishart, D.S. & Sykes, B.D. (1994) Chemical shifts as a tool for structure determination. *Methods Enzymol.* **239**, 363–392.
41. Metzler, W.J., Constanine, K.L., Friedrichs, M.S., Bell, A.J., Ernst, E.G., Lavoie, T.B. & Mueller, L. (1993) Characterization of the three-dimensional solution structure of human profilin: ^{1}H, ^{13}C, and ^{15}N NMR assignments and global folding pattern. *Biochemistry* **32**, 13818–13829.
42. Spera, S. & Bax, A. (1991) Empirical correlation between protein backbone conformation and ^{13}C nuclear magnetic resonance chemical shifts. *J. Am. Chem. Soc.* **113**, 5490.
43. Bagby, S., Harvey, T.S., Kay, L.E., Eagle, S.G., Inouye, S. & Ikura, M. (1994) Unusual helix-containing Greek keys in development-specific Ca^{2+}-binding protein S. ^{1}H, ^{15}N, and ^{13}C assignments and secondary structure determined with the use of multidimensional double and triple resonance heteronuclear NMR spectroscopy. *Biochemistry* **33**, 2409–2421.
44. Santoro, M.M. & Bolen, D.W. (1988) Unfolding free energy changes determined by the linear extrapolation method. 1. Unfolding of phenylmethanesulfonyl α-chymotrypsin using different denaturants. *Biochemistry* **27**, 8063–8068.
45. Wenk, M., Jaenicke, R. & Mayr, E.M. (1998) Kinetic stabilisation of a modular protein by domain interactions. *FEBS Lett.* **438**, 127–130.
46. Wenk, M. & Jaenicke, R. (1999) Calorimetric analysis of the Ca(2+)-binding betagamma-crystallin homolog protein S from

Myxococcus xanthus: intrinsic stability and mutual stabilization of domains. *J. Mol. Biol.* **293**, 117–124.
47. Teintze, M., Inouye, M. & Inouye, S. (1988) Characterization of calcium-binding sites in development-specific protein S of *Myxococcus xanthus* using site-specific mutagenesis. *J. Biol. Chem.* **263**, 1199–1203.
48. Barrick, D. & Baldwin, R.L. (1993) Stein and Moore Award address. The molten globule intermediate of apomyoglobin and the process of protein folding. *Protein Sci.* **2**, 869–876.
49. Kuwajima, K. (1996) The molten globule state of α-lactalbumin. *FASEB J.* **10**, 102–109.
50. Chamberlain, A.K. & Marqusee, S. (1998) Molten globule unfolding monitored by hydrogen exchange in urea. *Biochemistry* **37**, 1736–1742.
51. Eliezer, D., Yao, J., Dyson, H.J. & Wright, P.E. (1998) Structural and dynamic characterization of partially folded states of apomyoglobin and implications for protein folding. *Nat. Struct. Biol.* **5**, 148–155.
52. Kay, M.S. & Baldwin, R.L. (1996) Packing interactions in the apomyglobin folding intermediate. *Nat. Struct. Biol.* **3**, 439–445.
53. Schulman, B.A. & Kim, P.S. (1996) Proline scanning mutagenesis of a molten globule reveals non-cooperative formation of a protein's overall topology. *Nat. Struct. Biol.* **3**, 682–687.
54. Wu, L.C. & Kim, P.S. (1998) A specific hydrophobic core in the α-lactalbumin molten globule. *J. Mol. Biol.* **280**, 175–182.
55. Griko, Y.V. (2000) Energetic basis of structural stability in the molten globule state: α-lactalbumin. *J. Mol. Biol.* **297**, 1259–1268.
56. Koshiba, T., Yao, M., Kobashigawa, Y., Demura, M., Nakagawa, A., Tanaka, I., Kuwajima, K. & Nitta, K. (2000) Structure and thermodynamics of the extraordinarily stable molten globule state of canine milk lysozyme. *Biochemistry* **39**, 3248–3257.
57. Fink, A.L., Calciano, L.J., Goto, Y., Kurotsu, T. & Palleros, D.R. (1994) Classification of acid denaturation of proteins: intermediates and unfolded states. *Biochemistry* **33**, 12504–12511.